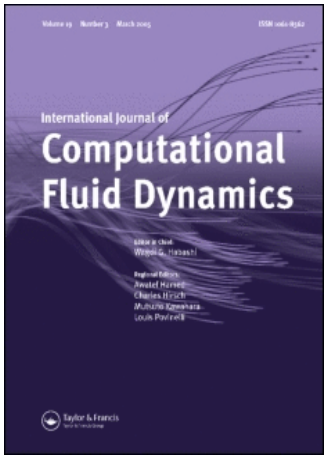

International Journal of Computational Fluid Dynamics
Publication details, including instructions for authors and subscription information:
http://www.informaworld.com/smpp/title~content=t713455064

An improved three-dimensional model for interface pressure calculations in free-surface flows

Ali Jafari [a]; Ebrahim Shirani [a]; Nasser Ashgriz [a]
[a] Department of Mechanical and Industrial Engineering, University of Toronto, Toronto, Ont., Canada

Online Publication Date: 01 February 2007
To cite this Article: Jafari, Ali, Shirani, Ebrahim and Ashgriz, Nasser (2007) 'An improved three-dimensional model for interface pressure calculations in free-surface flows', International Journal of Computational Fluid Dynamics, 21:2, 87 - 97
To link to this article: DOI: 10.1080/10618560701440915
URL: http://dx.doi.org/10.1080/10618560701440915

International Journal of Computational Fluid Dynamics, Vol. 21, No. 2, February 2007, 87–97

An improved three-dimensional model for interface pressure calculations in free-surface flows

ALI JAFARI†, EBRAHIM SHIRANI‡ and NASSER ASHGRIZ*

Department of Mechanical and Industrial Engineering, University of Toronto, Toronto, Ont., Canada M5S 3G8

(Received 4 May 2006; revised 16 December 2006; in final form 1 May 2007)

A three-dimensional method for the calculation of interface pressure in the computational modeling of free surfaces and interfaces is developed. The methodology is based on the calculation of the pressure force at the interfacial cell faces and is mainly designed for volume of fluid (VOF) interface capturing approach. The pressure forces at the interfacial cell faces are calculated according to the pressure imposed by each fluid on the portion of the cell face that is occupied by that fluid. Special formulations for the pressure in the interfacial cells are derived for different orientations of an interface. The present method, referred to as pressure calculation based on the interface location (PCIL), is applied to both static and dynamic cases. First, a three-dimensional motionless drop of liquid in an initially stagnant fluid with no gravity force is simulated as the static case and then two different small air bubbles in water are simulated as dynamic cases. A two-fluid, piecewise linear interface calculation VOF method is used for numerical simulation of the interfacial flow. For the static case, both the continuum surface force (CSF) and the continuum surface stress (CSS) methods are used for surface tension calculations. A wide range of Ohnesorge numbers and density and viscosity ratios of the two fluids are tested. It is shown that the presence of spurious currents (artificial velocities present in case of considerable capillary forces) is mainly due to the inaccurate calculation of pressure forces in the interfacial computational cells. The PCIL model reduces the spurious currents up to more than two orders of magnitude for the cases tested.

Also for the dynamic bubble rise case, it is shown that using the numerical solver employed here, without PCIL, the magnitude of spurious currents is so high that it is not possible to simulate this type of surface tension dominated flows, while using PCIL, we are able to simulate bubble rise and obtain results in close agreement with the experimental data.

Keywords: Free-surface flows; Surface tension; Volume-of-fluid (VOF) method; Spurious currents; Continuum surface force (CSF); Continuous surface stress (CSS)

1. Introduction

In simulation of interfacial flows with fixed mesh, determination of the interface pressure and surface tension has been one of the most troublesome and challenging issues. Surface tension forces appear in equations by imposing a jump condition across the interface. This condition is difficult to apply numerically and has been the center of attention by many researchers (Williams *et al.* 1998, Kang *et al.* 2000, Jamet *et al.* 2002, Meier *et al.* 2002, Renardy and Renardy 2002, Ye *et al.* 2004). There are two distinct ways of including surface tension in the overall solution. The first category of methods such as the boundary condition capturing method by Kang *et al.* (2000) and also the sharp-interface method by Ye *et al.* (2004) applies capillary force as a boundary condition along the free surface. In this method, the interface is considered to be a discontinuity separating the two fluids. The field equations are solved separately for each phase on a fixed grid, while interface is accounted for by forming irregular computational cells to match the interface shape. Since, the field equations in each fluid need to be coupled between different phases, and explicitly linked with the interfacial conditions, this method is computationally expensive, although it gives accurate results for the case of a static drop in static equilibrium.

The second approach for modeling surface tension forces, which is much more popular and has been

*Corresponding author. Tel.: + 1-416-946-3408. Fax: + 1-416-978-7753. Email: ashgriz@mie.utoronto.ca
†Email: ajafari@mie.utoronto.ca
‡Permanent address: Department of Mechanical Engineering, Isfahan University of Technology, Isfahan, Iran. Email: eshirani@cc.iut.ac.ir

International Journal of Computational Fluid Dynamics
ISSN 1061-8562 print/ISSN 1029-0257 online © 2007 Taylor & Francis
http://www.tandf.co.uk/journals
DOI: 10.1080/10618560701440915

extensively used in the volume of fluid (VOF) (Scardovelli and Zaleski 1999) and level set (Sussman *et al.* 1994, Sussman and Smereka 1997) methods, is to solve a single set of equations throughout the whole domain and simply add the capillary forces to the Navier–Stokes equations as an additional body force (Brackbill *et al.* 1992). In this method, since the location of interface is not usually known *a priori*, the surface tension force is applied as a body force in the vicinity of the interface over a few cells. This method is computationally more affordable than the other methods; however, there are still some serious problems to be addressed. The total surface tension force over a closed surface (surface integral) equals to zero, however, it cannot be ensured in most numerical techniques. This is due to the fact that interface is not as sharp as in the sharp interface method (Ye *et al.* 2004) and thus the surface integrals due to capillary forces can neither be evaluated accurately nor strictly obeyed to equal zero for closed surfaces.

In volume tracking techniques such as the VOF method, the two most widely used methods of this type are continuum surface force (CSF) and continuum surface stress (CSS) models. The CSF model reformulates surface tension into an equivalent volumetric force F^{st} as follows (Brackbill *et al.* 1992):

$$F_v^{\mathrm{st}} = \sigma\kappa\delta_s\mathbf{n} = \sigma\kappa\mathbf{n}\frac{|\nabla F|}{[F]} \tag{1}$$

where F is the volume fraction which is zero where only fluid 2 exists and is one where only fluid 1 exits and between zero and one if the cell contains a portion of the free surface (interfacial cell), σ is the coefficient of the surface tension, $[F]$ denotes the difference between the maximum and the minimum values of F (which is 1 here), $\mathbf{n}$ is the unit normal to the surface, δ_s is the delta function and κ is the surface curvature which can be written as:

$$\kappa = \nabla\cdot\mathbf{n} = -\nabla\cdot\frac{\nabla F}{|\nabla F|} \tag{2}$$

The above model produces an artificial acceleration in the lighter fluid when the density ratio of the two fluids is large. This acceleration is the main source of producing the so called "spurious" or "parasitic" currents (artificial velocities due to an inaccurate representation of surface tension terms and the associated pressure jump). Brackbill *et al.* (1992) and Kothe *et al.* (1996) recommended the addition of a density scaling factor in order to reduce the adverse effects of such acceleration. They proposed the following equation instead of equation (1):

$$F_v^{\mathrm{st}} = \sigma\kappa\delta_s\mathbf{n} = \sigma\kappa\mathbf{n}\frac{|\nabla F|}{[F]}\frac{\rho}{[\rho]} \tag{3}$$

where ρ is the local value of density obtained by the following equation (local value of viscosity is obtained using a similar relation):

$$\rho = \rho_2 + F(\rho_1 - \rho_2) \tag{4}$$

and $[\rho]$ is the difference between the density of the heavier and the lighter fluids. The density correction term (the second fraction in equation (3)) is added to correct the force in the momentum equation. This dampens the acceleration of the lighter fluid in the cells near the interface that contain small amounts of heavier fluid. The newly added fraction is not directly obtained from any conservation law, but it is merely postulated. We will later examin the effectiveness of this term and will compare it with our PCIL model.

Surface tension is then incorporated into the flow equations simply as a component of the body force. In the CSS method, the volumetric force used in the CSF method is converted into stress form. In this model, the effects of capillary force are presented as a stress tensor $\mathbf{T}$, which is tangential to the interface and is given by:

$$\mathbf{T} = -\sigma(\mathbf{I} - \mathbf{n}\otimes\mathbf{n})\delta_s \tag{5}$$

where $\mathbf{I}$ is the Kronecker symbol tensor δ_{ij} and δ_s is delta function. Then, the capillary force is written as:

$$\mathbf{F}^{\mathrm{st}} = -\nabla\cdot\mathbf{T} \tag{6}$$

The equivalent volume force derived from the CSS model can be written as (Lafaurie *et al.* 1994):

$$F_v^{\mathrm{st}} = \sigma\nabla\cdot\left(|\nabla F|\mathbf{I} - \frac{\nabla F\otimes\nabla F}{|\nabla F|}\right) \tag{7}$$

Discretization of surface tension forces according to the CSF or CSS methods can lead to the formation of spurious currents. These currents are strongly growing vortical flows in the transition region. In fact, neither of these models produces very accurate numerical solution in capillary dominated fluid problems (Rudman 1998, Meier *et al.* 2002). In problems where the surface tension forces dominate the viscous forces, the spurious currents can cause interface oscillations and, in some cases, deform or destroy the interface.

2. Model formulation

We present a new simple method for calculating surface tension force, which we will refer to as the pressure calculation based on the interface location (PCIL) (Shirani *et al.* 2005). We show that by an accurate implementation of the pressure forces at the interfacial cells, it is possible to eliminate a significant portion of the spurious currents.

For illustration, we show a two-dimensional interfacial cell (figure 1), in which fluid 1 (heavier fluid) and fluid 2 are separated by an interface line (plane in 3D). If we write the force balance, e.g. for the left face, the average pressure on the left face can be written in terms of

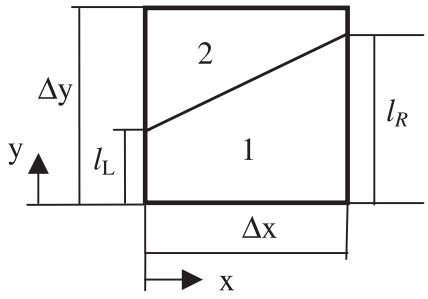

Figure 1. An interfacial cell described based on the volume of the fluids.

pressures of fluids 1 and 2 and an additional non-dimensional parameter (H_L) representing the interface location:

$$p_L = p_{2L} + H_L(p_{1L} - p_{2L}) \quad \text{where} \quad H_L = \frac{l_L}{\Delta y} \tag{8}$$

This parameter (H_L) shows the ratio of the left cell face area occupied by fluid 1 to the total left face's area. In general, for all cell faces, one can write:

$$p = p_2 + H(p_1 - p_2) \tag{9}$$

Therefore, the volumetric surface force using the CSF model, defined in equation (1), based on the PCIL model (using equation (9)) becomes:

$$F_v^{st} = H\sigma\kappa\mathbf{n}\frac{|\nabla F|}{[F]} \tag{10}$$

Applying the PCIL to the CSS model yields:

$$F_v^{st} = H\sigma\nabla\cdot\left(|\nabla F|\mathbf{I} - \frac{\nabla F\otimes\nabla F}{|\nabla F|}\right) \tag{11}$$

The code SURFER (Lafaurie *et al.* 1994) is modified and used for implementation and testing of the PCIL method. The details of the numerical method based on piecewise linear interface calculation VOF and projection method for a semi-implicit Navier–Stokes solver, which have been used in this code, are given in Lafaurie *et al.* (1994) and Gueyffier *et al.* (1999). Two different continuum methods, namely the CSF (Brackbill *et al.* 1992) and the CSS (Lafaurie *et al.* 1994) methods, for modeling the interfacial tension are used in this work. The Poisson equation is solved using the multigrid method. We have examined the performance of these methods with and without the PCIL model.

3. Calculation of "H" in three dimensions

The value of H on each side of a cell depends on the location of the interface at the same cell. In the piecewise linear interface calculation VOF method (Gueyffier *et al.* 1999, Scardovelli and Zaleski 1999) which is used in this work, the interface is approximated by a plane of appropriate inclination in each cell. This type of VOF method provides a second order approximation of real interface. The straight planes are not connected to each other at the cell faces. That is, the interface at each cell is determined independently of the neighboring planes and their ends need not necessarily be connected at the cell faces. Each plane is determined so that it is perpendicular to an interface normal vector, and it divides the cell surface into two regions that matches the given F for the cell. So the interface normal vector $\mathbf{n}$, which is a unit vector perpendicular to the interface pointing to fluid 2, is to be determined for each cell. Interface unit normal $\mathbf{n}$ is determined from the gradients of F by using the values of F for the cell under consideration and its 26 neighboring cells in a stencil of $3 \times 3 \times 3$. That is:

$$\mathbf{n} = \frac{\nabla F}{|\nabla F|} \tag{12}$$

More details about obtaining unit normal vector can be found in Meier *et al.* (2002). Once the normalized unit vector $\mathbf{n}$ is calculated (with components n_x, n_y and n_z in x, y and z directions, respectively), a plane is positioned perpendicular to it in such a way that it matches with the value of F in the cell.

Let n_1, n_2 and n_3 be the minimum, middle and maximum values of $|n_x|$, $|n_y|$ and $|n_z|$. Thus:

$$\begin{aligned} n_1 &= \min\big(|n_x|, |n_y|, |n_z|\big), \\ n_3 &= \max\big(|n_x|, |n_y|, |n_z|\big), \\ n_2 &= |n_x| + |n_y| + |n_z| - n_1 - n_3 \end{aligned} \tag{13}$$

These are components of $\mathbf{n}$ along the x_1, x_2 and x_3 axes (note that x_1, x_2 and x_3 axes are not necessarily x, y and z axes, respectively). Let d denote the distance of origin to the plane interface. The intercepts of this plane on the x_1, x_2 and x_3 axes are (figure 2):

$$s_1 = \frac{d}{n_1}, \quad s_2 = \frac{d}{n_2}, \quad s_3 = \frac{d}{n_3} \tag{14}$$

Note that since $n_1 \le n_2 \le n_3$, therefore $s_1 \ge s_2 \ge s_3$.

In order to match the volume fraction, we need to find the value of d for which the volume of the cubic cell beneath the plane is equal to F. Also, to reduce the number of cases that need to be considered, we only consider the

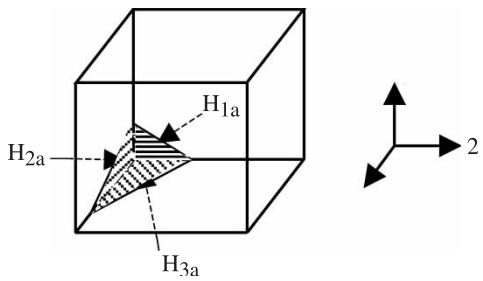

Figure 2. An interfacial cell and some of "s" and "H" components.

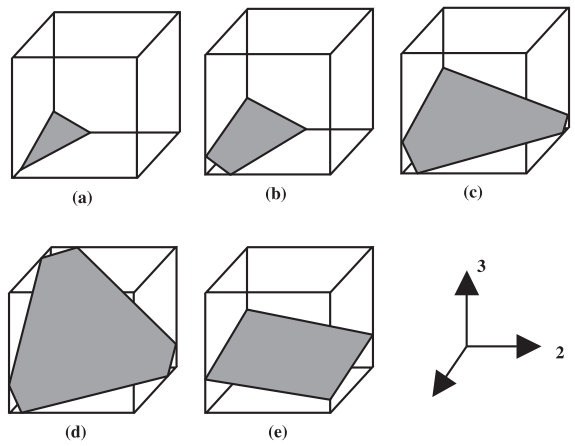

Figure 3. Possible intersection conditions for a plane intersecting a unit cube for $F < 0.5$: (a) triangular section, (b) quadrilateral section *A*, (c) pentagonal section, (d) hexagonal section and (e) quadrilateral section *B*.

cases when $F < 0.5$ in detail. For $F > 0.5$, the sign of **n** is reversed and the interface position is adjusted to match the volume fraction 1-*F*. Hence, in the rest of this section the volume fraction used, *F*, will be less than 0.5. As shown in figure 3, there are five possible cases where the interface shape is triangular, quadrilateral section *A*, pentagonal section, hexagonal section and quadrilateral section *B* (Littlefield and Oden 2000).

For the triangular section (case (a)), we have:

$$6n_1n_2n_3F < n_1^3 \tag{15}$$

and the vertical distance of interface from origin *d* is:

$$d = (6Fn_1n_2n_3)^{1/3} \tag{16}$$

For the quadrilateral section *A* (case (b)), we have:

$$n_1^3 \leq 6n_1n_2n_3F < n_2^3 - (n_2 - n_1)^3 \tag{17}$$

and *d* becomes:

$$d = \frac{n_1}{2} + \left[\left(2n_2n_3F - \frac{n_1^2}{12}\right)\right]^{1/2} \tag{18}$$

For the pentagonal section (case (c)),

$$n_2^3 - (n_2 - n_1)^3 \leq 6n_1n_2n_3F < n_3^3 - (n_3 - n_1)^3 - (n_3 - n_2)^3 \text{ and } n_1 + n_2 > n_3 \tag{19}$$

or

$$n_2^3 - (n_2 - n_1)^3 \leq 6n_1n_2n_3F < (n_1 + n_2)^3 - n_2^3 - n_1^3 \text{ and } n_1 + n_2 \leq n_3 \tag{20}$$

and

$$d^3 + (d - n_1)^3 - (d - n_2)^3 - 6n_1n_2n_3F = 0 \tag{21}$$

For the hexagonal section (case (d)),

$$n_3^3 - (n_3 - n_1)^3 - (n_3 - n_2)^3 \leq 6n_1n_2n_3F \text{ and } n_1 + n_2 > n_3 \tag{22}$$

and

$$d^3 + (d - n_1)^3 - (d - n_2)^3 - (d - n_3)^3 - 6n_1n_2n_3F = 0 \tag{23}$$

For the quadrilateral section *B* (case (e)),

$$(n_1 + n_2)^3 - n_2^3 - n_1^3 \leq 6n_1n_2n_3F \text{ and } n_1 + n_2 > n_3 \tag{24}$$

and

$$d = Fn_3 + \frac{1}{2}(n_1 + n_2) \tag{25}$$

Note that for cases (c) and (d), *d* is calculated by Newton–Raphson iteration. Using the value of *d*, we can determine the values of s_1, s_2 and s_3 from equation (14) for all cases. Since the interface is approximated by a plane of appropriate inclination in each cell, the side areas of each cell which is in contact with fluid 1 can have different shapes like triangle, trapezium, etc depending on different cases (figure 3). The sides of these shapes can be expressed in terms of s_1, s_2 and s_3. Note that in some cases, s_1, s_2 and s_3 exceed 1 and become larger than unit cube's sides. For example, for the triangular section (case (a)), all the values of s_1, s_2 and s_3 are less than 1, but in the quadrilateral section A (case (b)), $s_1 > 1$, but others remain less than 1. The *H* values in three dimensions (H_{1a}, H_{1b}, H, H_{2b}, H_{3a} and H_{3b}) are the areas of these shapes that can be written in terms of s_1, s_2 and s_3 as shown in table 1. Note that the 1, 2 and 3 subscripts refer to directions determined from equation (13), "*a*" indices indicate closer sides to the origin in each direction, while "*b*" indices indicate other sides (figure 2).

Now, we can determine the values of H_L, H_R, H_T, H_B, H_F and H_D (*H* values for left, right, top, bottom, front and back sides) for each cell in terms of s_1, s_2 and s_3. Using equation (13) and also considering the sign of normal vector, we can find the corresponding values of and H_x, H_y and H_z. An example is shown in figure 4, in which we assumed $n_x = n_1$, the values of H_L and H_R for left and right sides can be determined in different conditions depending on the cell volume fraction *F* and the interface direction.

Except for the cell faces at the boundaries of the computational domain, each cell face is adjacent to two other cells. Thus, two H_f values are calculated for any face f, one from each of the interior cell faces. For example, for the left side of cell (*i*,*j*,*k*), we have $H_{L,i,j,k}$ and for the right side of cell (*i*-1,*j*,*k*), we have $H_{R,i-1,j,k}$. If the interface lines are not connected to each other, the two values of H_f may be different. Based on several different trials, we have found that a simple averaging method (i.e. using the averaged *H* value for that face from two adjacent cells) works well to eliminate this problem. This prevents the

Table 1. H Values for different cases in terms of s_1, s_2 and s_3.

Case H	(a)	(b)	(c)	(d)	(e)
H_{1a}	$\frac{s_2 s_3}{2}$	$\frac{s_2 s_3}{2}$	$\frac{s_3}{2}\left(\frac{2s_2-1}{s_2}\right)$	$2(s_2+s_3)-\frac{s_2}{s_3}-\frac{s_3}{s_2}-s_2s_3-1$	$\frac{s_3}{2}\left(\frac{2s_2-1}{s_2}\right)$
H_{1b}	0	$\frac{s_2 s_3}{2}\left(\frac{s_1-1}{s_1}\right)^2$	$\frac{s_2 s_3}{2}\left(\frac{s_1-1}{s_1}\right)^2$	$\frac{s_2 s_3}{2}\left(\frac{s_1-1}{s_1}\right)^2$	$\frac{s_3}{2}\left(\frac{2s_2-1}{s_2}\right)\left(\frac{s_1-1}{s_1}\right)$
H_{2a}	$\frac{s_1 s_3}{2}$	$\frac{s_3}{2}\left(\frac{2s_1-1}{s_1}\right)$	$\frac{s_3}{2}\left(\frac{2s_1-1}{s_1}\right)$	$2(s_1+s_3)-\frac{s_1}{s_3}-\frac{s_3}{s_1}-s_1s_3-1$	$\frac{s_3}{2}\left(\frac{2s_1-1}{s_1}\right)$
H_{2b}	0	0	$\frac{s_1 s_3}{2}\left(\frac{s_2-1}{s_2}\right)^2$	$\frac{s_1 s_3}{2}\left(\frac{s_2-1}{s_2}\right)^2$	$\frac{s_3}{2}\left(\frac{2s_1-1}{s_1}\right)\left(\frac{s_2-1}{s_2}\right)$
H_{3a}	$\frac{s_1 s_2}{2}$	$\frac{s_2}{2}\left(\frac{2s_1-1}{s_1}\right)$	$2(s_1+s_2)-\frac{s_1}{s_2}-\frac{s_2}{s_1}-s_1s_2-1$	$2(s_1+s_2)-\frac{s_1}{s_2}-\frac{s_2}{s_1}-s_1s_2-1$	1
H_{3b}	0	0	0	$\frac{s_1 s_2}{2}\left(\frac{s_3-1}{s_3}\right)^2$	0

creation of internal pressure forces as source terms in the flow field.

Note that the calculation of H_f does not need extra operation in the VOF method, since the values of n_x, n_y and n_z, s_1, s_2 and s_3 are already calculated during the interface reconstruction process.

4. Results and discussion

To investigate the effects of using PCIL model on the prediction of surface tension forces, we have conducted two cases. The first case is a static drop and the second case is a bubble starting to rise in a liquid medium.

4.1 Static case

We have tested the PCIL method on the temporal evolution of a three-dimensional stationary liquid drop in another fluid without gravity, nearly similar to that of Williams *et al.* (1998). The drop radius, r, the fluid densities, ρ_1 and ρ_2, the viscosities, μ_1 and μ_2 and the surface tension coefficient, σ, are the main physical variables (subscript 1 stands for the drop and 2 for the surrounding fluid). We have also investigated the effects of variation of physical properties (i.e. density, viscosity and surface tension coefficient) on the flow field. If the computed pressure gradient at the drop interface does not balance with the surface tension force, spurious currents will be present. These currents tend to grow with time. The drop radius is taken as $0.25L$, where L is the domain length in the x-direction and is set equal to one. A $32 \times 32 \times 32$ uniform mesh, which is a typical resolution for simulation of interfacial flows, and a time step of $\Delta t = 10^{-5}$ s is chosen for all of the stationary droplet calculations.

From the dimensional analysis, the above mentioned physical properties are grouped into three non-dimensional parameters:

$$Oh_1 = \frac{\mu_1}{\sqrt{r\rho_1\sigma}}, \quad \frac{\rho_1}{\rho_2} \quad \text{and} \quad \frac{\mu_1}{\mu_2} \tag{26}$$

where Oh_1 is the (liquid) Ohnesorge number based on the properties of fluid 1 contained in the drop. Following Popinet and Zaleski (1999) and Scardovelli and Zaleski (1999), for a constant radius drop and from the dimensional analysis, the velocity of spurious currents is only a function of the surface tension coefficient and viscosity, i.e. $u \sim \sigma/\mu$ and it is not a function of density. Thus, it is expected that as the density of the flow changes, the velocity of the spurious currents remains constant.

A wide range of values including the properties of water (fluid 1) and air (fluid 2) are used for the above parameters. The results are presented in terms of the norms of the velocity (mean values of the absolute velocity) and the maximum values of the velocity of the spurious currents as a function of various variables. Figure 5 shows the velocities of spurious currents (shown for the cross section of sphere) at $N = 2000$, where N is the number of time steps. The scale for the velocity vectors shown in all figures is the same. The results in this case are obtained for a water drop in air, i.e. $\rho_1/\rho_2 = 830.545$, $\mu_1/\mu_2 = 54.945$ and the Ohnesorge number based on the water properties (Oh_1) is 2.34×10^{-4}. Figure 6 shows the maximum and norm of spurious currents as a function of time for the CSS model with and without the PCIL model. Addition of the PCIL model drastically reduces the spurious currents

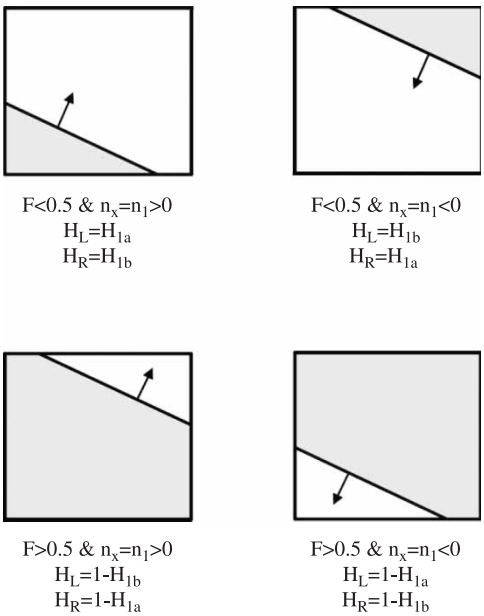

Figure 4. Typical representation of different cases for determining H values in an interfacial cell.

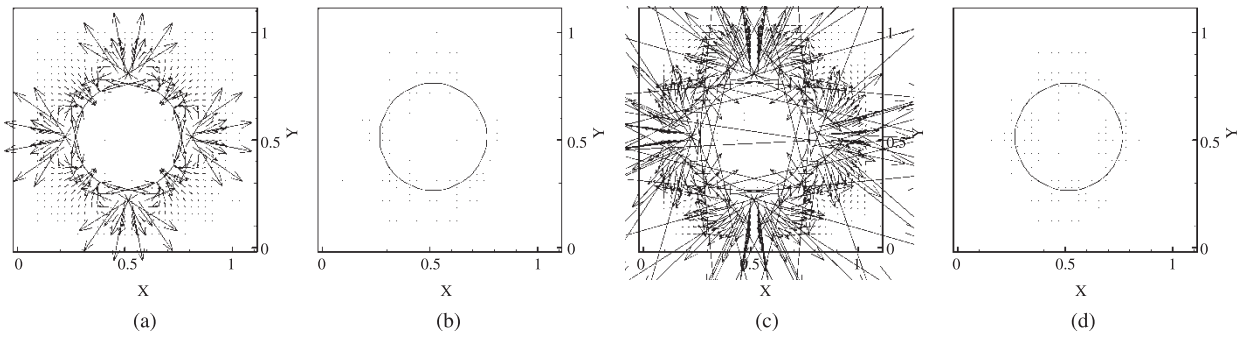

Figure 5. Spurious currents (shown for a slice of sphere) with the same velocity scales for (a) the CSS model, without the PCIL model, (b) CSS with PCIL, (c) CSF without PCIL and (d) CSF with PCIL.

(by more than two orders of magnitude). For the CSF model (figure 7), we have compared the results with and without the density correction factor, the second fraction in equation (3). As can be seen, the velocity of spurious currents produced by both CSS and CSF models are reduced by orders of magnitudes when the PCIL model is used. In the CSF model, when the PCIL model and the density ratio correction are not used, the spurious currents are larger than that of the CSS model. Once the density correction ratio is added, the spurious currents magnitude becomes smaller than that of CSS. By implementing the PCIL model, without density ratio correction, the velocities of the spurious currents drop by about two orders of magnitude. Note that in all the cases studied, the spurious currents still tend to increase with time. From figure 7, it can clearly be seen that the implementation of the PCIL factor is enough to reduce the spurious currents and there is no need to implement the density ratio correction in addition to the PCIL. Therefore, the PCIL model is a better alternative to the density ratio correction, which is a somewhat heuristic relation.

Effects of fluid properties in the form of density and viscosity ratios and Ohnesorge number are considered here. Figure 8 shows the maximum and the norm velocities of spurious currents as a function of density ratio for both CSS and CSF models, respectively. Results for cases with and without the PCIL model are presented. The viscosity ratio (μ_1/μ_2) is 54.945 and $Oh_1 = 2.34 \times 10^{-4}$ (equivalent to that of a water droplet in air). This figure shows that as the density ratio increases, the magnitude of the spurious velocities increases much more slowly with density ratio for the corrected pressure forces, while it increases rapidly when the correction is not applied. This evolution of velocity in the corrected version is in agreement with the dimensional analysis, which indicates that $u \sim \sigma/\mu$ and it should not be a function of density. It has been recorded by other researchers (e.g. see Gueyffier *et al.* 1999) that by increasing the density ratio, the spurious velocities grow and thus other methods cannot get reasonable results for high density ratios. However, it is possible to get reasonable results for high density ratios using PCIL.

Figure 9 shows the maximum and norm velocities of the spurious currents as a function of liquid Ohnesorge number (Oh_1) for the CSS and CSF models. Results for both cases with and without the PCIL model are presented. In this figure, the density ratio (ρ_1/ρ_2) is 830.545 and the viscosity ratio (μ_1/μ_2) is 54.945. It is shown that the

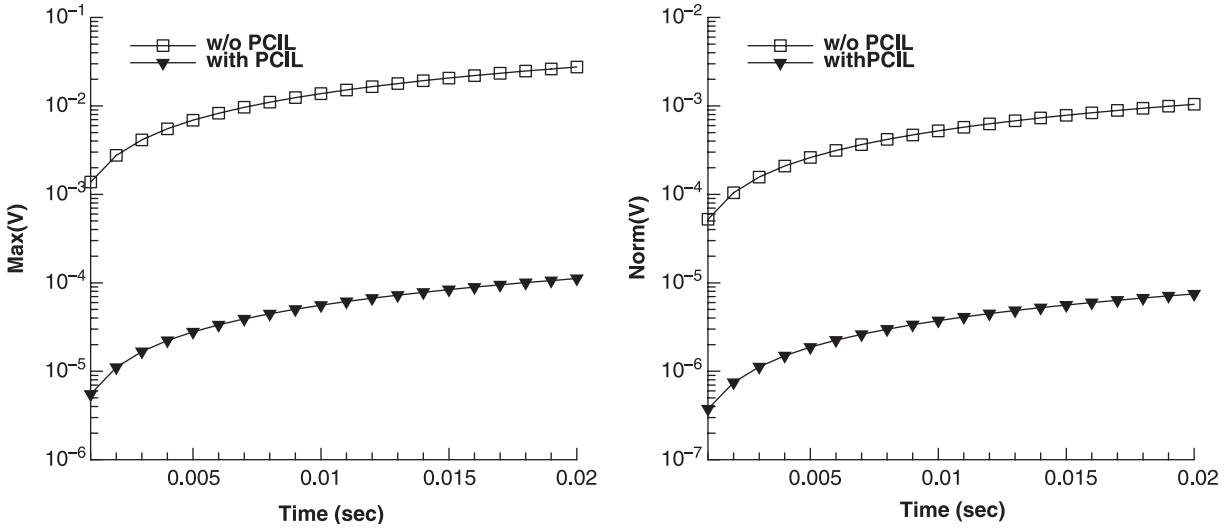

Figure 6. Maximum (left) and norm (right) spurious velocities vs. time for CSS model.

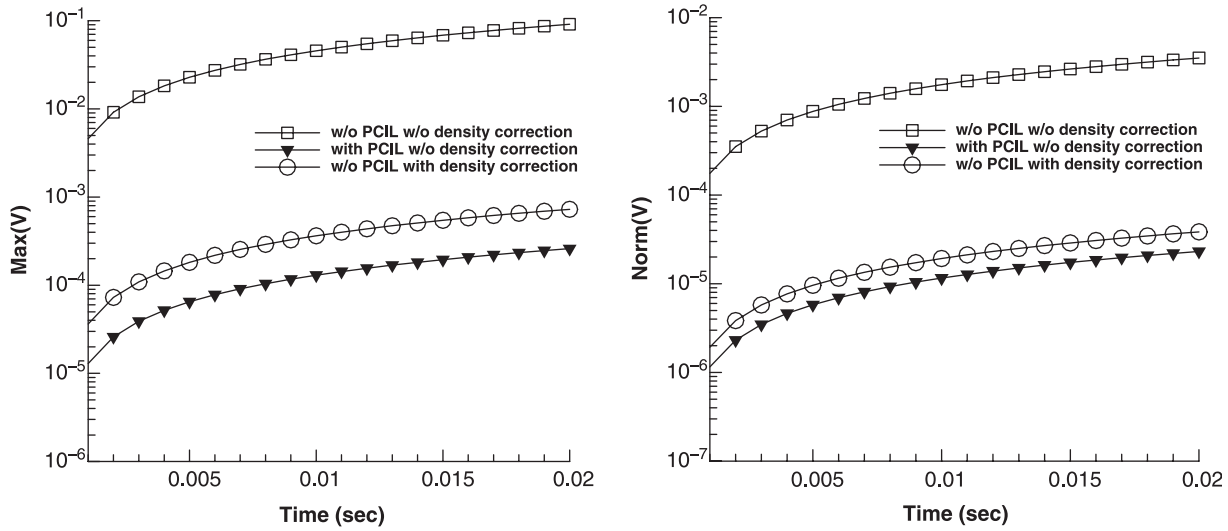

Figure 7. Maximum (left) and norm (right) spurious velocities vs. time for the CSF model without and with density correction term.

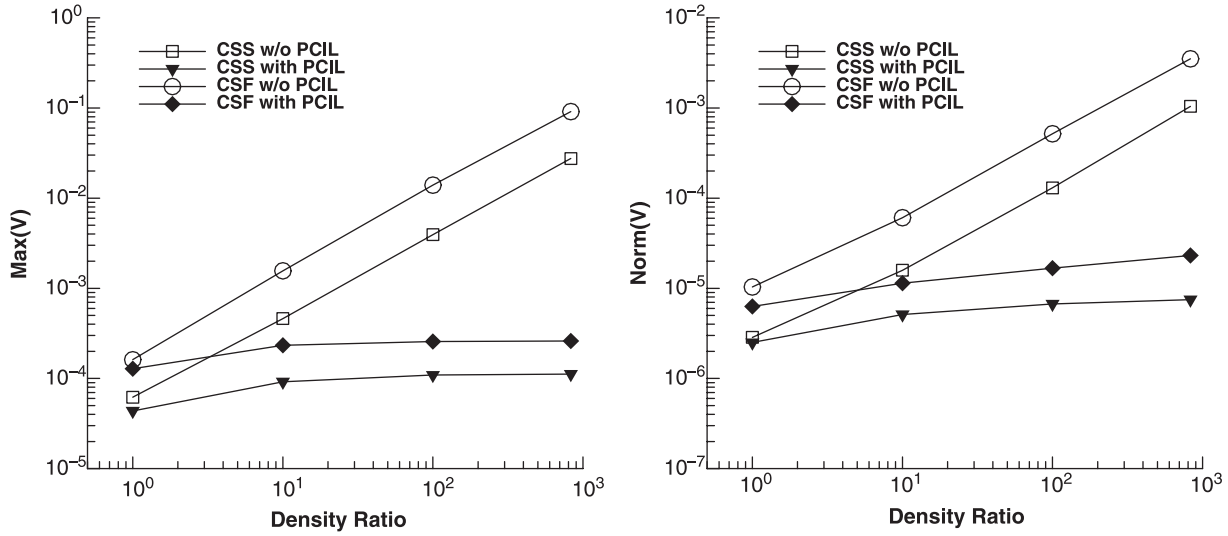

Figure 8. Maximum (left) and norm (right) spurious velocities as a function of density ratio.

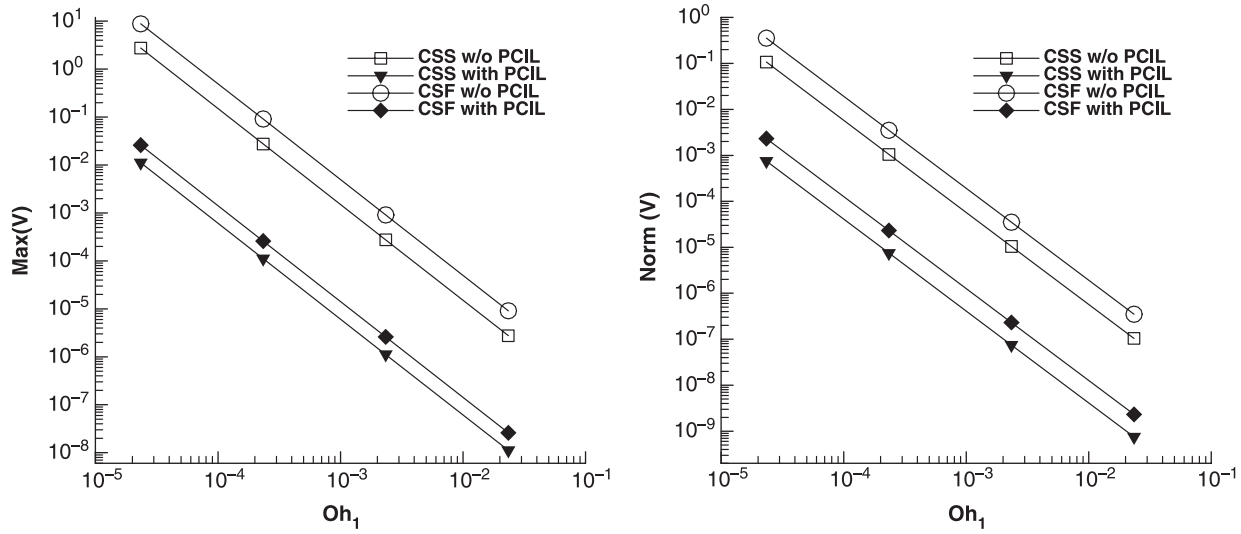

Figure 9. Maximum (left) and norm (right) spurious velocities as a function of Ohnesorge number.

spurious velocities decrease by two orders of magnitude when the PCIL is used. As Oh_1 increases, the spurious velocities decrease by a power law. The variation of the velocity with Oh_1 is also in agreement with the dimensional analysis which indicates $u \sim \sigma/\mu$.

Figure 10 shows the maximum and the norm velocities of the spurious currents as a function of viscosity ratio for the CSS and the CSF models, respectively. Results for both cases with and without the PCIL model are presented. In this figure, the density ratio (ρ_1/ρ_2) is 830.545 and $Oh_1 = 2.34 \times 10^{-4}$. Here, μ_1 has been changed and in order to keep Oh_1 constant, the surface tension coefficient is changed accordingly. It is shown that the spurious velocities decrease by more than two orders of magnitude when PCIL model is applied. As the viscosity ratio increases, the spurious velocities increase by a power law. This variation is also in agreement with the dimensional analysis which indicates that $u \sim \sigma/\mu$, see (Popinet and Zaleski 1999, Scardovelli and Zaleski 1999).

To further assess the accuracy of this method, we have determined the mean pressure difference between inside and outside the droplet summing over the liquid and gas cells, respectively. This pressure jump should agree with the analytical value $2\sigma/R$ for a spherical droplet. Thus, the pressure jump error is defined as:

$$\text{error} = \frac{\left(\overline{p_1} - \overline{p_2}\right) - 2\sigma/R}{2\sigma/R} \tag{27}$$

where, $\overline{p_1}$ and $\overline{p_2}$ are the mean values of pressure inside and outside of the drop. Note that if the pressures $\overline{p_1}$ and $\overline{p_2}$ were calculated exactly, the value of error would be zero. This error remained below 3% for all cases which is comparable to Meier's *et al.* (2002) results.

Also, it should be noted that the PCIL method has symmetry, i.e. it works for all cases regardless of where the fluids one and two are located. To ensure this, we have repeated the calculations for a static bubble instead of a drop for the two-dimensional version of PCIL and observed similar improvements.

4.2 Dynamic case

Most of the studies in reduction of spurious currents only have used static drop or static bubble as their reference test case. In those cases, the effects of surface tension are dominated while inertia and gravity effects are neglected. To further assess the efficiency of the PCIL method, we have used a dynamic but surface tension dominated case. In this case, a small spherical air bubble starts to rise in water from stationary condition, influenced by buoyancy, surface tension and viscous effects. This is a notoriously difficult problem for the VOF based methods and even for the front tracking methods (Shin *et al.* 2005) especially since the density ratio is very high (around 830) and small bubble size creates large surface tension forces which is difficult to tackle. The reason is that even small discrepancy between capillary force and pressure gradient may destabilize the solution (Shin *et al.* 2005).

Comparing the three approaches (VOF, level set and front tracking), the level set methods have the least difficulty dealing with surface tension dominated problems such as the rise of small gas bubbles in liquid (Sussman and Smereka 1997). However, most level set methods still suffer from mass loss problems and even after many efforts to improve the mass conservation properties (Bourlioux 1995, Sussman and Fatemi 1999, Enright *et al.* 2002, van der Pijl *et al.* 2005), they tend to introduce non-physical curvature fluctuations. This is because the above mentioned correction methods are local.

On the other hand, the front tracking method (Unverdi and Tryggvason 1992) has shortcomings dealing with merging and breakup of interfaces, as well as surface tension dominated flows (Shin *et al.* 2005). The VOF methods have been the most popular method in the interfacial flow simulation community. However, despite

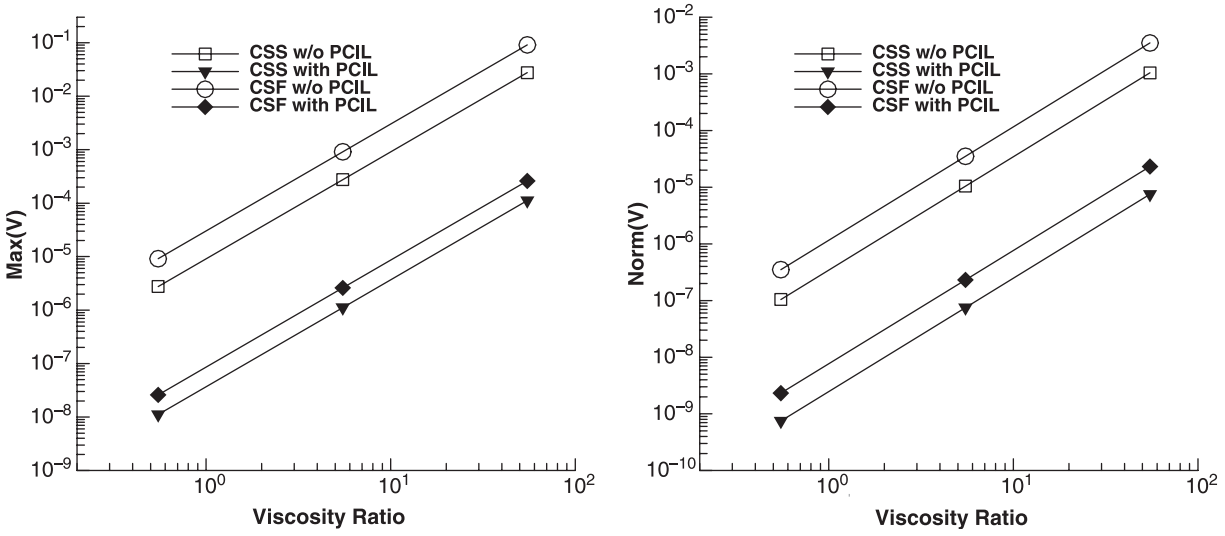

Figure 10. Maximum (left) and norm (right) spurious velocities as a function of viscosity ratio.

their mass conservation and natural treatment of merging and breakup, they have difficulty dealing with surface tension dominated flows.

There has been a number of previous bubble simulations using VOF methods (Tomiyama *et al.* 1993, Chen *et al.* 1999, Meier 1999, Meier *et al.* 2002, van Wachem and Schouten 2002), but only a few of them (Meier 1999, Meier *et al.* 2002) have been able to simulate very small bubbles in the order of 1 mm in diameter and with such high density ratios. Most VOF implementations still suffer from non-physical oscillations and instabilities due to handling of surface tension dominated flows. The PCIL methodology is designed to alleviate such problems.

According to equation (7.3) and (figure 7) of Clift *et al.* (1978), the terminal rise velocity U_T of small air bubbles in pure water at room temperature can be determined using the following experimental correlation:

$$U_T = \sqrt{2.14\sigma/\rho d_e + 0.505 g d_e} \tag{28}$$

where d_e is the diameter of a sphere of equal volume (or initial bubble diameter as we start simulation from spherical bubble). This correlation is also in accordance with the results of other similar experimental studies (Martin and Chandler 1982, Tomiyama *et al.* 1998). Also, according to figure 2 of Clift *et al.* (1978), a bubble of diameter $D = 1.5$ mm is in the spherical shape regime while for larger bubble with diameter $D = 3$ mm, it is approximately in the ellipsoidal regime. We choose to simulate these two different sized bubbles as our dynamic test case.

For the simulations, the three-dimensional space has the size of $5D \times 5D \times 20D$ in the x, y and z directions, respectively. However, because of symmetry, only a quarter of the domain is solved for most cases and, therefore, the number of grid points are $32 \times 32 \times 256$ (13 cells per diameter approximately). The CFL number is chosen to be 0.2 in order to obtain accurate results.

In some surface tension-dominated flow simulations, since the spurious currents are dominating the solution at high density ratio (e.g. in water–air system), some researchers use lower density ratios to circumvent this problem. For example, Gueyffier *et al.* (1999) used a gas density six times higher than air density to avoid such parasitic solution. Here, we have used the actual densities of air and water. The CSS surface tension model is used here.

The bubble shapes for small and large bubbles are shown in figures 11 and 12, respectively. The left column shows the shape without using the PCIL model and the right column with the PCIL method. Note that in the left columns, the initial bubble shape (at time $t = 0$) is not shown for clarity. For both cases, we see that without using PCIL, the bubble undergoes severe non-physical deformations because of problems in calculating surface tension forces. Similar non-physical bubble deformations are observed by Meier *et al.* (2002) (see figure 6 of Meier *et al.*) for CSF model. Also, Shin *et al.* (2005) simulated a similar problem using front tracking method and reported chaotic parasitic currents as well as "mass loss". The parasitic velocities grow until they become able to deform the bubble dramatically. This large deformation happens earlier for smaller bubbles, i.e. at time 0.4 ms, while for the larger bubble it takes around 3 ms for spurious currents to grow and cause significant bubble deformations. In fact, at these times, the magnitude of spurious velocities are so high that they cause time step to decrease by orders of

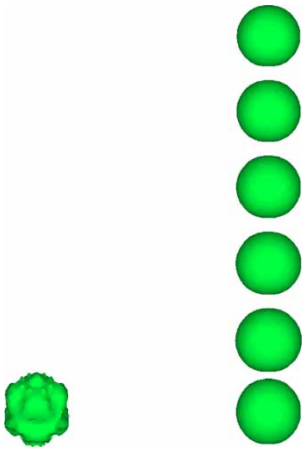

Figure 11. The bubble shape for $D = 1.5$ mm without PCIL after 0.4 ms (left) and with H at times 0, 14, 21, 27, 34 and 40 ms (right).

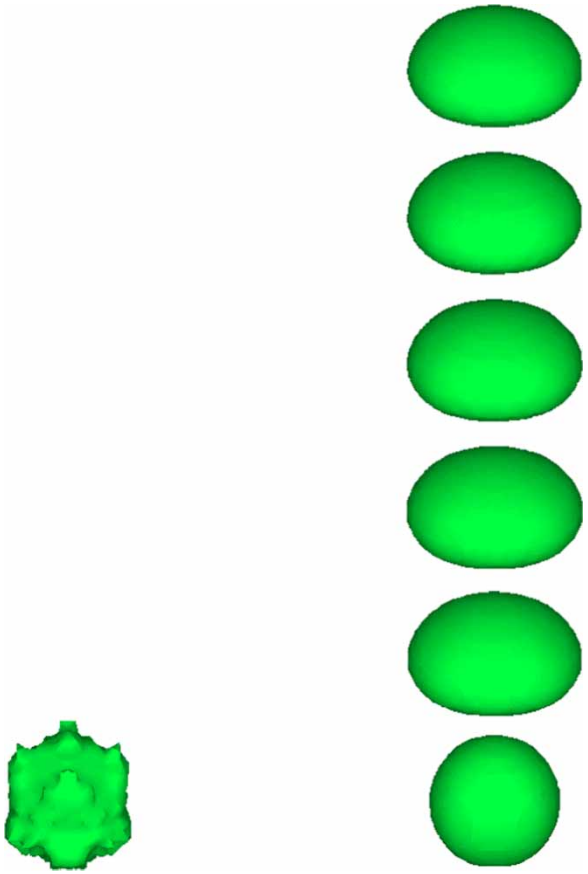

Figure 12. The bubble shape for $D = 3$ mm without PCIL after 3 ms (left) and with PCIL at times 0, 25, 40, 55, 70 and 85 ms (right).

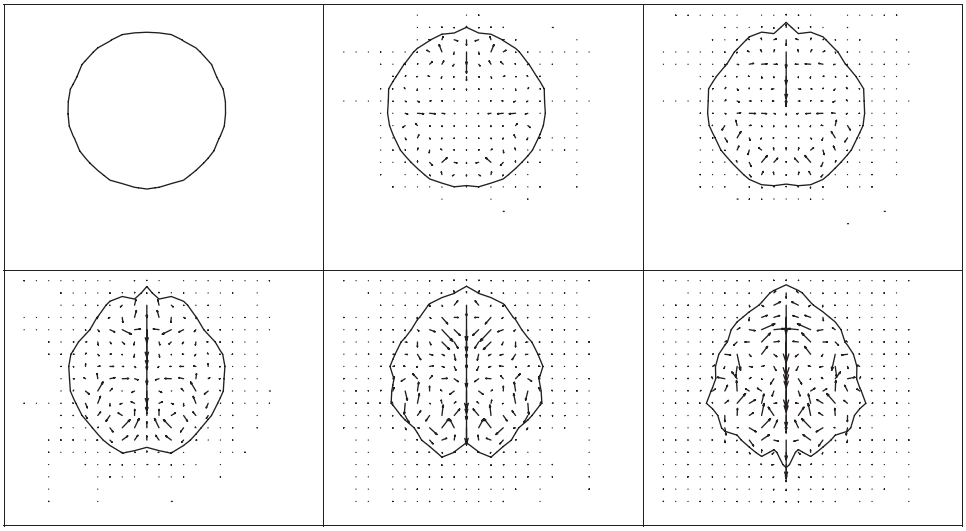

Figure 13. Evolution of bubble shape and velocity vectors for a 3 mm bubble without PCIL at times 0, 1.5, 1.875, 2.25, 2.625 and 3 ms, respectively (the bubble cross-section is shown).

magnitude and it is not possible to continue simulation to get a long time solution yet this solution is not acceptable because of erroneous bubble deformation. The evolution of the shape and velocity of the larger bubble is shown in figure 13 at times before 3 ms. As it is observed, the spurious currents start at the upper side of the bubble and grow fast in time, such that they deform the bubble surface considerably.

The right columns of figures 11 and 12 show that using PCIL, the bubble maintains its shape and the spurious forces have reduced dramatically so that the bubble shapes are in accordance with experimental results. Compared to Meier's (1999) results, for larger bubbles we get similar results while for smaller bubbles, our results are better since there is no non-physical deformation and the bubble stays spherical as the experiments suggest.

In addition to bubble shapes, the calculated rise velocities for both bubbles are compared to the experimental data (straight lines) in figure 14. The solid lines correspond to smaller bubble while the dotted lines belong to a larger bubble. Good agreement between numerical and experimental data (Clift *et al.* 1978, Tomiyama *et al.* 1998) is observed. For the smaller bubble ($D = 1.5$ mm), since the bubble stays spherical and there is less numerical error, the bubble rise velocity is much closer to the experimental value than Meier's (1999) data.

It should be noted that in simulation of free-surface flows, in addition to the surface tension method used, there are other factors affecting the quality and robustness of the numerical simulations. These include pressure-velocity coupling and pressure solution algorithm. For example, Takahira *et al.* (2003) presented an improved level set method for gas–liquid flows. They reported that using preconditioning BiCGSTAB for the solution of Poisson's equation, their method works well for density ratios up to 10,000:1. However, using multigrid method the iteration did not converge for density ratios higher than 20:1. This is an indication of the importance of the pressure–velocity coupling and solution schemes on the accuracy of the results. The improvements can be gained using PCIL under any other solution methodology. Here, the results of the original methodology for the case of small bubble rise were not acceptable. After applying PCIL, the results are in good agreement with the experimental correlations.

5. Conclusion

A three-dimensional method for the calculation of the pressure force at the interfacial cells for VOF based methods is derived and presented in detail. In this method (PCIL), first the intersections of an interface with the computational cell faces are determined. The area of a cell

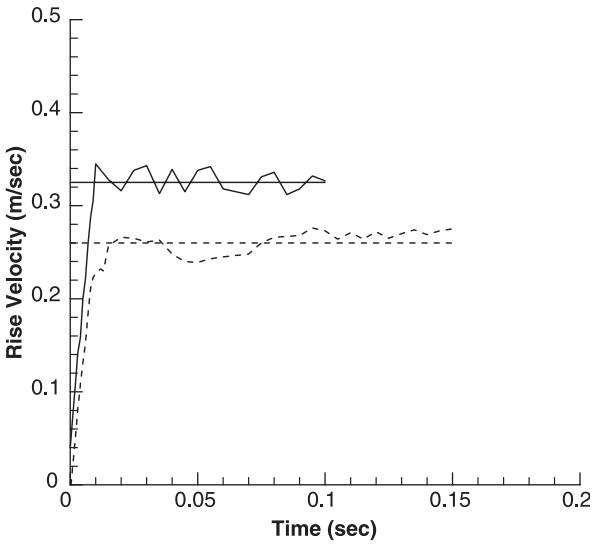

Figure 14. Rise velocities versus time of simulated small air bubbles in air in comparison to the experimental U_T from equation (28) (horizontal lines). Solid lines correspond to $d = 1.5$ mm and dotted lines belong to $d = 3$ mm bubble.

face which is in contact with the heavier fluid is normalized with the cell face area to obtain a factor H (between 0 and 1). Then, the two H values obtained from the cells on both sides of each internal cell face are averaged. Finally, the capillary force used in momentum equation is corrected by multiplying it by the factor H determined for each cell face.

This method is applied to both static and dynamic cases. For the static case, evolution of a still drop in a motionless fluid is solved numerically. It is shown that the spurious currents decrease by more than two orders of magnitude. The influences of Ohnesorge number, density and viscosity ratios of the two fluids on the spurious currents are examined. It is shown that the spurious currents grow with increasing surface tension coefficient and are suppressed with increasing viscosity. Increasing the density ratio has little effect on the spurious currents in the present model. However, the spurious currents drastically increase with the density ratio when PCIL is not used (original surface tension models). Although the spurious currents are reduced by several orders of magnitude when corrected surface tension force is used, there are still some currents in the flow.

Also, two challenging dynamic cases of air bubbles rising in water have been simulated. It is shown that using PCIL, we are able to simulate bubble rise and obtain results (bubble shape and rise velocity) in close agreement with the experimental data. For the case of a smaller bubble, the spherical and smooth shape of the bubble demonstrates the accuracy and robustness of this method for surface tension dominated flows.

Acknowledgements

This work was supported by Natural Sciences and Engineering Research Council of Canada (NSERC), and Materials and Manufacturing Ontario (MMO).

References

Bourlioux, A., *A Coupled Level-set Volume-of-fluid Algorithm for Tracking Material Interfaces*, pp. 15–22, 1995 (Sixth Int'l Symposium on Computational Fluid Dynamics, IV: Lake Tahoe, NV).

Brackbill, J.U., Kothe, D.B. and Zemach, C., A continuum method for modeling surface tension. *J. Comput. Phys.*, 1992, **100**, 335–354.

Chen, L., Garimella, S.V., Reizes, J.A. and Leonardi, E., The development of a bubble rising in a viscous liquid. *J. Fluid Mech.*, 1999, **387**, 61–96.

Clift, R., Grace, J.R. and Weber, M.E., *Bubbles, Drops and Particles*, 1st ed., 1978 (Academic Press: London).

Enright, D., Fedkiw, R., Ferziger, J. and Mitchell, I., A hybrid particle level set method for improved interface capturing. *J. Comput. Phys.*, 2002, **183**, 83–116.

Gueyffier, D., Li, J., Nadim, A., Scardovelli, R. and Zaleski, S., Volume-of-fluid interface tracking with smoothed surface stress methods for three-dimensional flows. *J. Comput. Phys.*, 1999, **152**, 423–456.

Jamet, D., Torres, D. and Brackbill, J.U., On the theory and computation of surface tension: the elimination of parasitic currents through energy conservation in the second-gradient method. *J. Comput. Phys.*, 2002, **182**, 262–276.

Kang, M., Fedkiw, R.P. and Liu, X., A boundary condition capturing method for multiphase incompressible flow. *J. Sci. Comput.*, 2000, **15**(3), 323–360.

Kothe, D.B., Rider, W.J., Mosso, S.J. and Brock, J.S., Volume tracking of interfaces having surface tension in two and three dimensions. *AIAA Paper*, 96–0859, 1996.

Lafaurie, B., Nardone, C., Scardovelli, R., Zaleski, S. and Zanetti, G., Modelling merging and fragmentation in multiphase flows with SURFER. *J. Comput. Phys*, 1994, **113**, 134–147.

Littlefield, D. and Oden, J.T., *Implementation of Adaptive Mesh Refinement into an Eulerian Hydrocode*, TICAM Report No. ERDC MSRC/PET, 2000 (University of Texas at Austin: TX, USA).

Martin, W.W. and Chandler, G.M., The local measurement of the size and velocity of bubbles rising in liquids. In *Mechanics and Physics of Bubbles in Liquids*, edited by L. van Wijngaarden, 1982 (Nijhoff Publications).

Meier, M., *Numerical and Experimental Study of Large Steam-air Bubbles Injected in a Water Pool*, Dissertation no. 13091, 1999 (Swiss Federal Institute of Technology: Zurich, Switzerland).

Meier, M., Yadigaroglu, G. and Smith, B.L., A novel technique for including surface tension in PLIC-VOF methods. *Eur. J. Mech. B/Fluids*, 2002, **21**, 61–73.

Popinet, S. and Zaleski, S., A front-tracking algorithm for accurate representation of surface tension. *Int. J. Numer. Meth. Fluids*, 1999, **30**, 775–793.

Renardy, Y. and Renardy, M., PROST: a parabolic reconstruction of surface tension for the volume-of-fluid method. *J. Comput. Phys.*, 2002, **183**, 400–421.

Rudman, M., A vomlue-tracking method for incompressible multifluid flows with large density variations. *Int. J. Numer. Meth. Fluids*, 1998, **28**, 357–378.

Scardovelli, R. and Zaleski, S., Direct numerical simulation of free surface and interfacial flow. *Annu. Rev. Fluid Mech.*, 1999, **31**, 567–603.

Shin, S., Abdel-Khalik, S.I., Daru, V. and Juric, D., Accurate representation of surface tension using the level contour reconstruction method. *J. Comput. Phys.*, 2005, **203**(2), 493–516.

Shirani, E., Ashgriz, N. and Mostaghimi, J., Interface pressure calculation based on conservation of momentum for front capturing methods. *J. Comput. Phys.*, 2005, **203**, 154–175.

Sussman, M. and Fatemi, E., An efficient, interface-preserving level set redistancing algorithm and its application to interfacial incompressible fluid flow. *SIAM J. Sci. Comput.*, 1999, **20**, 1165–1191.

Sussman, M. and Smereka, P., Axisymmetric free boundary problems. *J. Fluid Mech.*, 1997, **341**, 269–294.

Sussman, M., Smereka, P. and Osher, S., A level set approach for computing solutions to incompressible two-phase flow. *J. Comput. Phys.*, 1994, **114**, 146–159.

Takahira, H., Horiuchi, T. and Banerjee, S., *An Improved Three-dimensional Level Set Method for Gas–Liquid Two-Phase Flows*, 2003 (8th International Symposium on Gas-Liquid Two-phase Flows: Honolulu, HI, USA).

Tomiyama, A., Zun, I., Sou, A. and Sakaguchi, T., Numerical analysis of bubble motion with the VOF method. *Nucl. Eng. Design*, 1993, **141**, 69–82.

Tomiyama, A., Kataoka, I., Zun, I. and Sakaguchi, T., Drag coefficients of single bubbles under normal and microgravity conditions. *JSME Int. J. Ser B: Fluids Thermal Eng.*, 1998, **41**, 472–479.

Unverdi, S.O. and Tryggvason, G., A front-tracking method for viscous, incompressible, multi-fluid flows. *J. Comput. Phys.*, 1992, **100**, 25–37.

van der Pijl, S.P., Segal, A. and Vuik, C., A mass-conserving level-set method for modelling of multi-phase flows. *Int. J. Numer. Meth. Fluids*, 2005, **47**, 339–361.

van Wachem, B.G.M. and Schouten, J.C., Experimental validation of 3-D Lagrangian VOF model: bubble shape and rise velocity. *AIChE J.*, 2002, **48**(12), 2744–2753.

Williams, M.W., Kothe, D.B. and Puckett, E.G., *Accuracy and Convergence of Continuum Surface Tension Models*, 1998 (Thirteenth U.S. National Congress of Applied Mechanics: Gainesville, FL).

Ye, T., Shyy, W., Tai, C.F. and Chung, J.N., Assessment of sharp- and continuous-interface methods for drop in static equilibrium. *Comput. Fluids*, 2004, **33**, 917–926.